J. Fluid Mech. (2009), *vol.* 637, *pp.* 357–385.
doi:10.1017/S0022112009990681

Acoustic radiation from turbulent premixed flames

RAJESH RAJARAM AND TIM LIEUWEN†

Georgia Institute of Technology, 270 Ferst Drive, Atlanta, GA 30332, USA

(Received 10 March 2008; revised 4 June 2009; accepted 4 June 2009; first published online 24 September 2009)

Turbulent combustion processes are inherently unsteady and, thus, a source of acoustic radiation. While prior studies have extensively characterized their total sound power, their spectral characteristics are not well understood. This work investigates these acoustic spectral features, including the flame's low- and high-frequency characteristics and the scaling of the frequency of peak acoustic emissions. The spatiotemporal characteristics of the flame's chemiluminescence emissions, used as a marker of heat release fluctuations, were measured and used to determine the heat release spectrum, spatial distribution and spatial coherence characteristics. These heat release characteristics were then used as inputs to an integral solution of the wave equation and compared to measured acoustic spectra obtained over a range of conditions and burners and at several spatial locations. The spectral characteristics of the flame's acoustic emissions are controlled by two processes: the underlying spectrum of heat release fluctuations that are ultimately the combustion noise source, and the transfer function relating these heat release and acoustic fluctuations. An important result from this work is the clarification of the relative roles of these two processes in controlling the shape of the acoustic spectrum. This transfer function is primarily controlled by the spatiotemporal coherence characteristics of the heat release fluctuations which are, in turn, strongly influenced by burner configuration/geometry and operating conditions. Low-frequency acoustic emissions are controlled by the heat release spectrum essentially independent of flame geometry. Both the heat release spectrum and heat release-acoustic transfer function are important at intermediate and high frequencies. An important feature of the investigated geometry that controls the heat release phase dynamics is the high-velocity flow relative to the flame speed and anchored character of the flame. This leads to convection of flame sheet disturbances (i.e. heat release fluctuations) along the front that dominates the high frequency and peak frequency scaling of the flame's acoustic emissions.

1. Introduction

Turbulent combustion processes are inherently unsteady and, thus, a source of acoustic radiation. Noise emission occurs due to the unsteady expansion of reacting gases at the turbulent flame front. Locally, such an expansion appears as an unsteady creation of volume and, hence, as a distributed monopole source. Dowling (in Crighton *et al*., 1992) derived a wave equation describing noise production in a reacting flow that includes a variety of source terms associated with the direct flow noise itself, diffusive effects and direct and indirect combustion noise. As described by Dowling,

† Email address for correspondence: tim.lieuwen@aerospace.gatech.edu

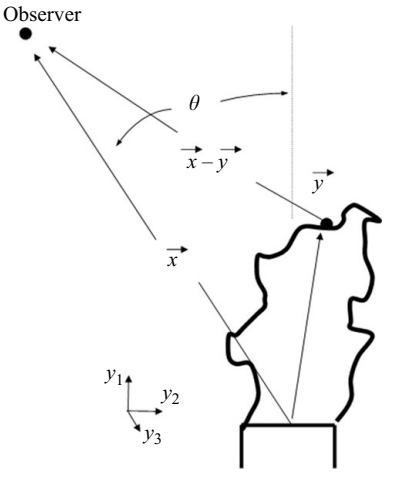

FIGURE 1. Schematic of turbulent flame and burner illustrating coordinate system used in the description of the acoustic field.

the direct combustion noise source is dominant in most cases, leading to a linear wave equation of the form

$$\frac{1}{c_0^2}\frac{\partial^2 p}{\partial t^2} - \nabla^2 p = -\frac{\partial}{\partial t}\left(\frac{\rho_0(\gamma-1)q}{\rho c^2}\right), \tag{1.1}$$

whose formal solution is

$$p'(\vec{x},t) = \frac{1}{4\pi}\frac{\partial}{\partial t}\int \left[\frac{\rho_0(\gamma-1)q}{\rho c^2}\right]_{t-|\vec{x}-\vec{y}|/c_0} \Big/ |\vec{x}-\vec{y}|\,\mathrm{d}\vec{y}, \tag{1.2}$$

where p, c, ρ, γ and q refers to the unsteady pressure, sound speed, fluid density, ratio of specific heats and rate of heat release per unit volume, respectively. The coordinate system that is used in the solution is illustrated in figure 1, where the points $\vec{y}$ describe the flame region and $\vec{x}$ denotes the measurement point. For situations where the number of reactant and product moles differ, an additional source term is also present, which is of much smaller magnitude for hydrocarbon–air flames (Truffaut *et al.* 1998).

The focus of this paper is on open, premixed flames (see Ihme, Pitsch & Bodony 2006, 2009 or Tam *et al.* 2005 for recent work on non-premixed flames) with a fixed composition, i.e. on the actual acoustic radiation from the flame itself, without the effects of enclosures, which lead to sound reflections, and entropy generated noise by the acceleration of temperature inhomogeneities through nozzles (Marble & Candel 1977; Muthukrishnan, Strahle & Neale 1978; Shivashankara 1978; Cumpsty 1979; Krejsa 1983). The heat release rate of a premixed flame with constant composition and flame speed is proportional to its surface area (Clavin & Siggia 1991) – fluctuations in fuel/air ratio due to imperfect mixing/acoustic pulsations (Cho & Lieuwen 2005), or stretch-induced flame speed variations (Wang *et al.* 2009), can also lead to heat release oscillations, effects which are outside of the scope of this investigation.

The problem of turbulent combustion noise, i.e. the conversion of turbulent velocity fluctuations into flame-generated (as opposed to flow generated) sound by distorting and wrinkling the turbulent flame front, can be decomposed into two distinct subproblems, as illustrated in figure 2. These are (*a*) the distortion and wrinkling

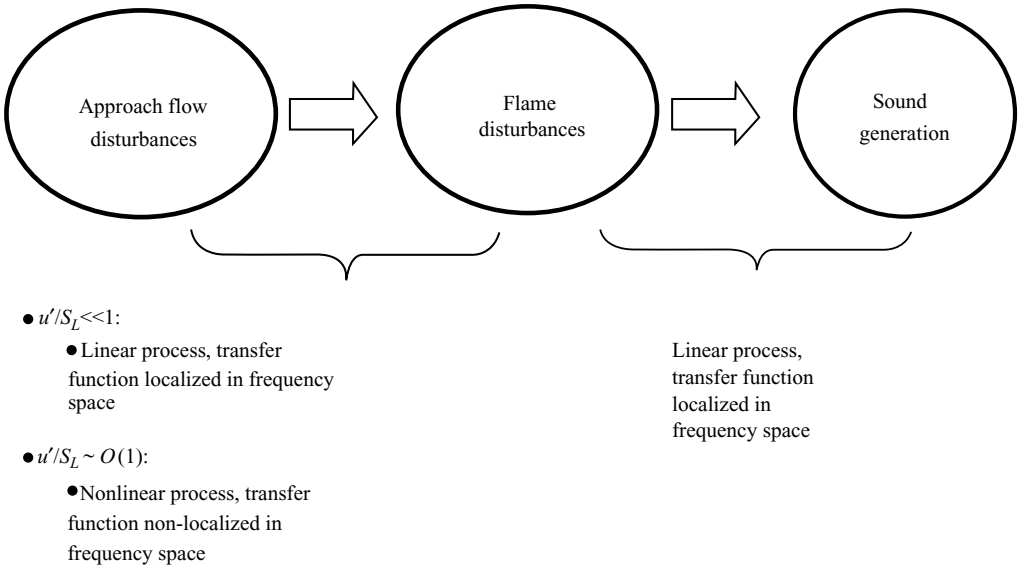

FIGURE 2. Physical processes involved in the conversation of turbulent velocity fluctuations into flame-generated sound within the linear acoustics approximation.

of the flame, resulting in a fluctuating flame area, and therefore heat release rate due to underlying turbulent velocity fluctuations, and (*b*) the generation of sound by these heat release fluctuations. The first subproblem is a turbulent combustion problem; it essentially generalizes analysis of the average turbulent flame mass burning rate (i.e. the turbulent flame speed), to consideration of its fluctuation characteristics as well. The second subproblem is an acoustics problem, which requires understanding the characteristics of the underlying sound source (the unsteady heat release), and the transfer function relating these source characteristics to the far-field sound field. This paper focuses on the second subproblem. That is, we do not attempt to characterize the transfer function between approach flow turbulent fluctuations and the flame's unsteady heat release rate. Rather, we measure these unsteady heat release characteristics and relate them to the measured acoustic emissions. Both of these subproblems are discussed in more detail throughout this section as we review prior literature on the combustion noise problem.

Consider first the overall sound power emitted by turbulent flames. This topic has received significantly more attention in the literature than on the spectral distribution of these emissions. For example, the data in Putnam (1976) and Kilham & Kirmani (1979) illustrate the combustion noise characteristics of various burners as a function of heat input, equivalence ratio and upstream turbulence levels. In general, these studies find that the total sound emissions from the flame scales with its overall heat release rate. At a fixed heat release rate, the dependence of its acoustic emissions upon air velocity, equivalence ratio, burner diameter and burner shape is more complex as the effects of these parameters, often coupled, could also depend on the turbulence characteristics of the incoming flow. In addition, a number of other studies have contributed to what is now a large empirical database of overall sound power level as a function of burner geometry, flow rate and reactant kinetic characteristics, e.g. see Giammar & Putnam (1972), Shivashankara (1974), Putnam (1976), Roberts & Leventhall (1973) and Strahle & Shivashankara (1974). These studies have also shown

that combustion noise is marginally directional (Smith 1961; Shivashankara 1974) due to distributed source effects (Lieuwen *et al.* 2006), convection and refraction (Strahle 1973; Dowling 1979). Results are summarized in reviews by Mahan (1984) and Dowling (in Crighton *et al.* 1992).

Most modelling studies are based upon the foundation laid by Lighthill (1952). However, the first explicit analysis and modelling of combustion noise appears to have been performed by Bragg (1963). While this model was heuristic in nature, it laid the foundation for subsequent, more rigorous analyses are given by Strahle (1971, 1978), Hassan (1974), Chiu & Summerfield (1973), Doak (1973), Dowling (in Crighton *et al.* 1992), Kotake (1975) and others. All these formulations lead to similar expressions for radiated sound power in terms of double spatial integrals of the unsteady heat release over the source region, e.g. see (1.3) below from Dowling (in Crighton *et al.* 1992), derived assuming that combustion occurs in a perfect gas at constant pressure:

$$P = \frac{\overline{p'^2}}{\rho_0 c_0} 4\pi|\vec{x}|^2 = \frac{(\gamma-1)^2}{4\pi\rho_0 c_0^5} \int\int \overline{\frac{\partial q}{\partial t}(\vec{y}_a, t - {}^{|\vec{x}-\vec{y}_a|}/_{c_0}) \frac{\partial q}{\partial t}(\vec{y}_b, t - {}^{|\vec{x}-\vec{y}_b|}/_{c_0})} \mathrm{d}^3\vec{y}_a \mathrm{d}^3\vec{y}_b. \quad (1.3)$$

The scaling of this equation is worked out in Dowling (in Crighton *et al.* 1992). As in other noise emission problems from spatially distributed random sources, evaluation of this integral requires modelling characteristics such as the correlation volume V_{corr} (Wäsle, Winkler & Sattelmayer 2005) or unsteady heat release and how these quantities scale with underlying turbulence parameters. Scaling these quantities is a more general turbulent combustion problem with many uncertainties, so most studies have used basic physical scaling, or semi-empirical correlations of these unknown parameters, in order to derive combustion noise models. For example, Hassan (1974) and Strahle & Shivashankara (1974) used empirical models for turbulence intensity and correlation length to estimate this integral, e.g. the latter study developed the result $P \propto F^{-0.4} S_L^{2.2} U_{ave}^{1.8} D^{3.4}$, where F is the fuel mass fraction, S_L is the laminar flame speed, U_{ave} is the mean velocity of the upstream flow and D is the burner diameter.

Having briefly discussed the total acoustic emissions from turbulent premixed flames, consider next their spectra, which has received significantly less attention. Typical combustion noise spectra are shown in figures 3–5. Data show that combustion noise is broadband in nature. Typical spectra of combustion noise emissions can exceed background noise levels for frequencies from 100 Hz to over 20 kHz (Briffa, Clark & Williams 1973; Ramohalli & Seshan 1983). The broadband spectrum of combustion noise typically increases with frequency, reaches a maximum at $f = f_{peak}$, and then rolls off towards the background noise level (see figure 5). Experiments generally show f_{peak} values occur in the 200–1000 Hz frequency range (Mahan 1984; Kotake & Takamoto 1987). Other data also indicate the presence of multiple peaks in the acoustic spectrum (Kumar 1975).

Studies have shown that while the acoustic spectrum can shift up or down in amplitude and left or right in frequency space, its basic shape remains essentially constant. There are analogies here to the jet noise problem (see Tam & Auriault 1999). This point can be seen from the four spectra shown in figure 3. These spectra were taken with different burner diameters, fuels and flow velocities and have magnitudes and peak frequencies that vary by an order of magnitude. However, when the magnitudes are scaled by the maximum power at f_{peak}, and the frequency is scaled by f_{peak}, the spectra collapse and are virtually indistinguishable (the only difference is for $f < f_{peak}$ in curve 4, due to non-negligible background noise levels at $f < 100$ Hz, see figure 5). Indeed, the measurements reported here show that the acoustic emissions

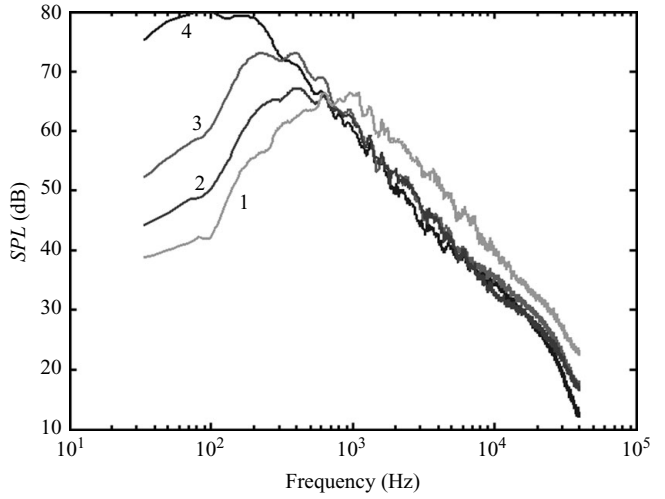

FIGURE 3. Four typical combustion noise spectra. Conditions are (1) $D = 6.4\,\text{mm}$, $U_{ave} = 40.2\,\text{m s}^{-1}$, Fuel = Acetylene, $\phi = 0.71$, $u'/U_{ave} = 0.8\%$, (2) $D = 10.9\,\text{mm}$, $U_{ave} = 21.8\,\text{m/s}$, Fuel = Acetylene, $\phi = 0.64$, $u'/U_{ave} = 1.5\%$, (3) $D = 17.3\,\text{mm}$, $U_{ave} = 17.4\,\text{m s}^{-1}$, Fuel = Propane, $\phi = 1.03$, $u'/U_{ave} = 11.5\%$, (4) $D = 34.8\,\text{mm}$, $U_{ave} = 9.6\,\text{m s}^{-1}$, Fuel = Natural Gas, $\phi = 0.95$, $u'/U_{ave} = 9.4\%$.

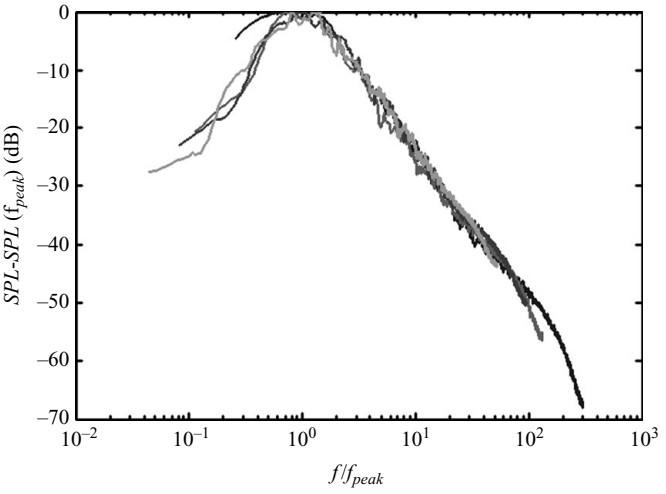

FIGURE 4. Same combustion spectra as shown figure 3, with normalized axes.

can be parameterized by a low-frequency spectral dependence given by f^{β}, a peak in the spectra at f_{peak}, and a high-frequency spectral decay as $f^{-\alpha}$, as shown in figure 5. The absolute magnitude of these spectral components scales with the total acoustic emissions from the flame. For example, Petela & Petela (1983) observed changes in the magnitude, but not the shape of the spectra with changes in overall heat release rate. Similar conclusions were drawn by Kotake & Takamoto (1987, 1990) who measured the influence of burner diameter and shape, flow velocity and turbulence intensity on the combustion noise spectrum. Given these observations, we frame the rest of this overview in terms of this parameterization of the acoustic spectrum (α, β and f_{peak}).

The frequency of peak amplitude emissions f_{peak} has been discussed extensively in the literature. As such, it is somewhat surprising that there is no consensus on

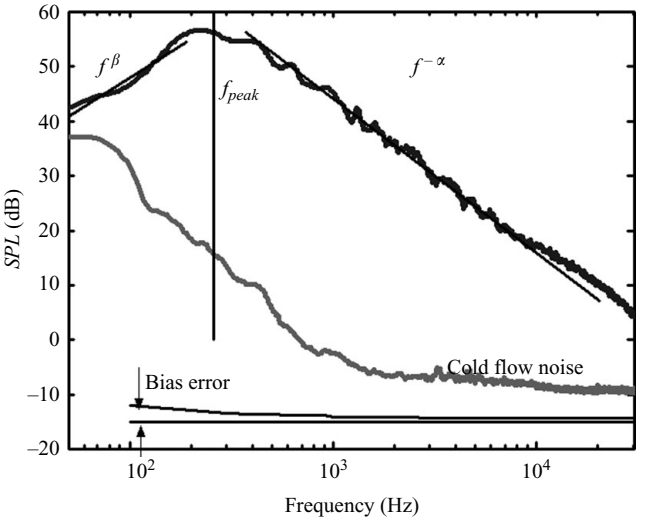

FIGURE 5. Typical combustion noise spectrum (natural gas fuelled, $D = 10.9$ mm, $U_{ave} =$ 21.8 m s^{-1}, $u'/U_{ave} = 1.5\%$, $\phi = 0.95$. Cold flow noise obtained with exhaust fans on. 'Bias Error' curve indicates uncertainties due to room reverberation effects.

its controlling parameters. A number of analyses have assumed a Strouhal number scaling for f_{peak}, based on burner diameter and jet exit velocity, similar to jet noise spectral scalings (Smith & Kilham 1963; Strahle & Shivashankara 1974). There have been related suggestions of a Strouhal number scaling based on the integral length scale and intensity of velocity fluctuations in the underlying turbulence (Strahle & Shivashankara 1974; Strahle 1983). Shortcomings of this type of scaling are highlighted in several studies that note that they implicitly assume that the combustion noise scales similarly to flow noise, and contain none of the known dependence of f_{peak} upon chemistry (Shivashankara, Strahle & Handley 1975; Kotake & Takamoto 1987; Rajaram & Lieuwen 2003). Other workers have suggested scalings that emphasize kinetic rates, such as flame speeds or characteristic kinetic times (Shivashankara *et al.* 1975; Stephenson & Hassan 1977; Abugov & Obrezkov 1978). For example, Abugov & Obrezkov (1978) suggested a Strouhal number scaling for f_{peak} based upon the burner diameter and the laminar flame speed. However, this scaling neglects the known influence of fluid mechanics, such as mean flow speed, upon peak frequency. For example, Smith & Kilham (1963) showed that the peak frequency increased with flow velocity when the chemical parameters were held constant. Shivashankara *et al.* (1975) also performed a regression of their data resulting in an empirical expression of the form $f_{peak} = 12.57 U_{ave}^{0.18} D^{-0.08} S_L^{0.52} F^{-0.69}$ that incorporates fluid mechanics (U_{ave}), geometry (D) and chemical kinetics (laminar flame speed S_L and fuel mass fraction F) influences upon f_{peak}.

Consider next the high-frequency characteristics of the acoustic spectrum $f^{-\alpha}$. A number of measurements have demonstrated the existence of an $f > f_{peak}$ spectral region with a power law dependence upon frequency (Huff 1986). Abugov & Obrezkov (1978) found that the spectrum exhibits a power law dependence with an exponent of $\alpha = 2.5$ over the 2–10 kHz frequency range. This power law behaviour was also found by Belliard (1997), who measured values in the range $2.4 < \alpha < 3.2$.

Modelling these spectral characteristics from first principles is challenging due to the highly nonlinear relationship between approach flow velocity disturbances and

the flame's heat release. To understand this, consider first the actual generation of sound by flame heat release disturbances, the second process shown in figure 2. This relationship is described by (2). For most problems of interest, this problem involves linear acoustics that are localized in frequency space, i.e. the heat release $\hat{Q}(f)$ and acoustic spectra $\hat{p}(f)$ are directly related through a transfer function which can be determined from (2). As shown in those equations, the key complexity associated with determining the relationship between $\hat{Q}(f)$ and $\hat{p}(f)$ is understanding the space–time correlation of the heat release characteristics. Indeed, measurement of these characteristics is a key part of this study in determining the acoustic spectrum.

Consider next the generation of flame disturbances by turbulent velocity fluctuations, the first process shown in figure 2. This is a turbulent combustion problem that has not been solved in general, but has been treated approximately in a number of analyses (Kerstein 1988; Aldredge 1991; Clavin & Siggia 1991; Lieuwen *et al.* 2006). This problem is highly nonlinear. For example, in the flame sheet limit, the flame dynamics are described by the G-equation, which relates the flame position (given by the $G=0$ contour) and surface area to the approach flow velocity disturbance field (Matalon & Matkowsky 1982) through the expression

$$\partial G/\partial t + \vec{u} \cdot \nabla G = S_L |\nabla G|. \tag{1.4}$$

It is well known that the parameter u'/S_L controls the degree of flame front wrinkling. In the $u'/S_L \ll 1$ limit, as also illustrated in figure 2, the relationship between flame area and turbulent velocity fluctuations is linear, implying that changes in spectra of velocity fluctuations will directly influence those of the flame area and, therefore, the radiated acoustic field. In contrast, the dynamics relating the velocity and flame area spectrum become increasingly nonlinear and non-local in frequency/wavenumber space with increasing u'/S_L, i.e. the heat release generated at some frequency f is a convolution of turbulent kinetic energy over a range of frequencies and length scales for highly turbulent flames where $u'/S_L \gg 1$.

Related points are discussed by Clavin (2000) and Clavin & Siggia (1991), who treated the combustion noise problem in the high u'/S_L limit. Their paper, while ultimately directed towards predicting the high frequency spectrum of combustion noise, more generally presents an approach for analysing the spectrum of flame surface area fluctuations. They presented a fractal analysis of the flame sheet, leading to a predicted power law dependence of the acoustic power spectrum of $\hat{P}(f) \sim f^{-5/2}$ (i.e. $\alpha = 5/2$) at frequencies corresponding to the inertial subrange in the turbulent velocity field, assuming Kolmogorov scaling and a $k^{-5/3}$ inertial subrange velocity wavenumber spectrum.

From the above discussion, two significant shortcomings in current understanding are evident. First, better understanding of the spectral characteristics of the acoustic emissions are needed. In particular, the lack of a consensus on scaling of f_{peak} constitutes a major deficiency in understanding. Second, better understanding of the relationship between the sound source (the unsteady heat release) and the radiated sound is needed.

Given these points, the objectives of this paper are three fold. The first objective is to generate a spectrally resolved database of acoustic radiation data from a turbulent premixed burner with well characterized inlet conditions in an anechoic environment. The anechoic environment is particularly critical as some of the spectral data in the literature is contaminated with either room reverberation effects or spurious approach flow noise. The second objective of this work is to obtain measurements of the spatiotemporal characteristics of the heat release fluctuations, in order to allow

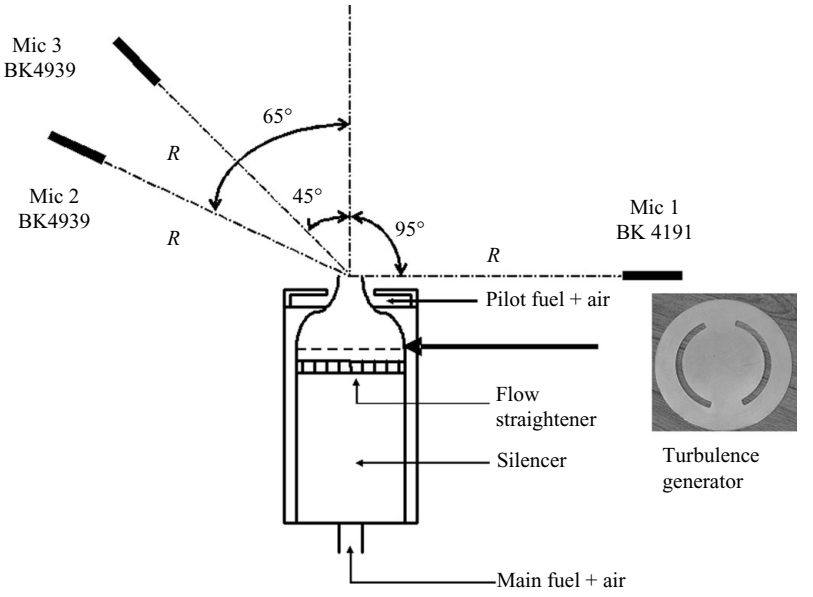

FIGURE 6. Schematic of the piloted burner with a picture of the turbulence generator and the position of the microphones.

direct comparisons of the acoustic and heat release spectrum. The final objective is to quantitatively relate these measured acoustic and heat release measurements in order to fully understand the flame's acoustic radiation. In particular, data, analysis and modelling of the total sound emissions from the flame, its spatial coherence, source distribution and spectral features are worked out and related to more fundamental features of the turbulent flame.

2. Experimental facility and instrumentation

The burner facility used for this study is shown in figure 6. The upstream flow enters a large plenum and flow silencer with a diameter of 101.6 mm, large compared to the burner exit diameter and the inlet flow pipes. The flow exits the silencer and passes through flow straighteners with exit turbulence levels well under 1 % of the mean flow velocity. The flow then enters the turbulence generator section, consisting of an axisymmetric version of the device described by Videto & Santavicca (1991). This turbulence generator consists of 1.27 mm thick plates with semicircular cut out slots of inner and outer diameter D_1 and D_2. Varying these values changes the turbulence level of each burner by altering the blockage area of the upstream flow. In this way, turbulence intensities ranging from about 0.5 %–13 % were obtained. Full geometric details of each generator are tabulated in Rajaram (2007).

After exiting the turbulence generator, the flow passes through a converging section down to the final nozzle diameter. Nozzle diameters of 34.8, 17.3, 10.9 and 6.4 mm were used, enabling contraction ratios of 8.5:1–256:1. These high contraction ratios led to very uniform exit velocity profiles with a thin boundary layer. The boundary layer thickness expectedly reduced with increasing contraction ratios. Note that data for our prior parametric investigation utilized a fully developed turbulent inflow profile (Rajaram & Lieuwen 2003).

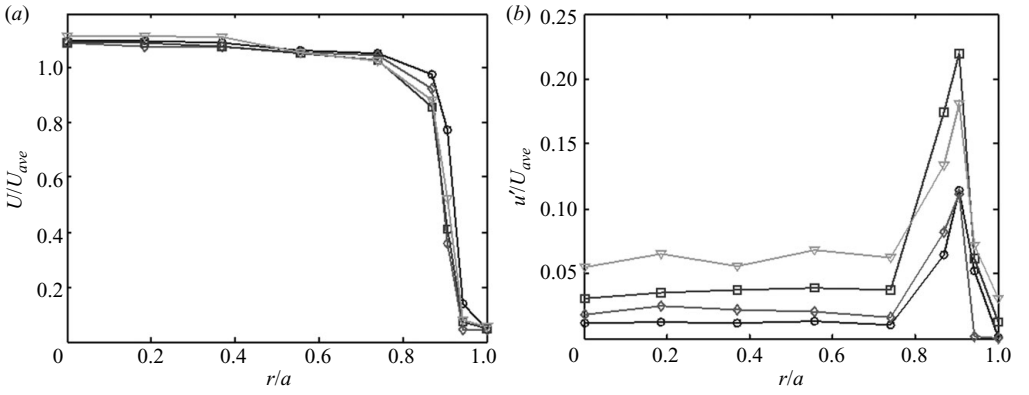

FIGURE 7. Mean and r.m.s. velocity profile for 10.9 mm burner for the case of $U_{ave} = 21.8$ m s^{-1} and blockage ratio of the turbulence generators being ○ 93.6 %, ◇ 94.2 %, □ 98.6 %, ▽ 99.1 %.

Velocity characteristics were measured using a constant temperature hotwire anemometer (CTA). The exit velocity profile was measured using a miniature straight probe with a wire diameter of 5 μm, held using a straight probe holder connected to a mechanical traverse. In addition, centreline velocity measurements were made using a 90° probe holder that eliminated probe holder interference for spectral measurements. The raw hotwire data were obtained at 80 kHz and low pass filtered at 30 kHz.

Figure 7 presents a typical result for the mean and fluctuating velocity with several turbulence generators. As noted above, the time averaged mean and fluctuating profiles are quite flat, except in the boundary layer. Note also the variation of turbulence intensity with changes in turbulence generator, as desired. Complete mean and fluctuating velocity profile results for all burner diameters are compiled in Rajaram (2007).

Figure 8 presents typical one-dimensional turbulent kinetic energy spectra at the burner centreline for several mean velocities. The spectra show a smooth roll-off with increasing frequency, and that there are no discrete peaks, as desired.

Burner exit velocities ranged from 5–48 m s^{-1}, allowing for exploration of a large range of u'/S_L values. The lower velocity limit was set by the requirement to maintain a turbulent flow; the Reynolds number $Re_D = U_o D/\nu > 10\,000$ for all data reported here. Its maximum value was set by the point where permanent, extinction induced holes in the flame occurred, which varies with fuel type and fuel/air ratio. These permanent holes occur near the flame tip and result in a significant portion of the fuel escaping and not burning. These flames have significantly different acoustic properties (Rajaram 2007), and are not considered here. Because this requirement limited the maximum Reynolds number to values less than 30 000, no distinctive inertial subrange is evident in the velocity spectra. Larger burner diameters which would allow for exploration of the higher Reynolds number regime were precluded by thermal load limitations of the anechoic chamber.

Stabilizing the flames at these high velocity's required a ring pilot flame around the outer circumference of the burner. The premixed pilot flame was fuel rich and supplied less than 5 % of the total fuel input into the flow. This pilot flow was introduced as a co-flow via a narrow slit around the burner 2.5 mm upstream of the burner exit point.

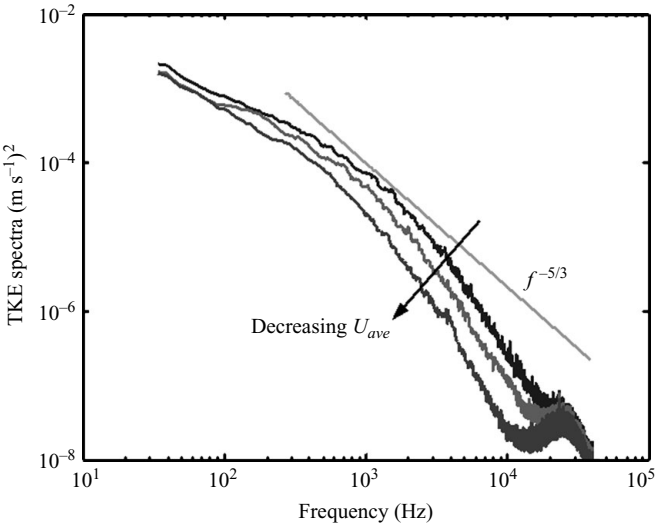

FIGURE 8. Typical spectra of one-dimensional turbulent kinetic energy ($D = 10.4$ mm, turbulence generator blockage ratio 93.6 % and $U_{ave} = 21.8$, 19 and 16.3 m s^{-1}.

Acoustic data were obtained with 3 Brüel & Kjær microphones that were placed 1.02 m from the burner at angles of $\theta = 45°, 65°$ and $90°$ from the vertical axis of the burner (see figure 6). The raw microphone signals were fed into Krohn-Hite Butterworth type band pass filters, set at lower and upper frequencies of 50 and 35 kHz, respectively, and then digitized with a 12-bit National Instruments data acquisition board (PCI-MIO-16E-1) at 80 kHz. The voltage limits of acquisition and microphone output gain were both adjusted with operating conditions to maximize the dynamic range of the system and minimize digitization errors.

The burner was placed inside an anechoic chamber for all acoustic measurements. Such a facility is essential for these data, as open room measurements lead to spurious peaks in the spectra due to reverberation effects. Indeed, it is very likely that some of the data in the literature containing multiple acoustic peaks in the spectra are due to these room reflections. Even for the data reported here, ripples in the spectrum are evident at low frequencies due to room reverberation effects. The external dimensions of the anechoic chamber are $4.11(\mathrm{L}) \times 3.22(\mathrm{W}) \times 3.58(\mathrm{H})$ m and fitted with 45.7 cm foam wedges. Air is recirculated through the chamber by baffled exhaust and inlet ducts. This environment significantly reduces the acoustic feedback provided in a reverberant acoustic field. The room temperature was allowed to reach steady state and remained constant throughout all test runs.

The characteristics of the anechoic chamber was characterized with the use of a 'point source' and the deviation from its $1/R^2$ law dependence in its far field (Ahuja 2003). Detailed results of chamber performance are in Rajaram (2007). They show that bias errors due to room reverberation effects are less than 1dB for $f > 400$ Hz and less than 0.5 dB for $f > 1250$ Hz. Background noise measurements were made in the quiescent environment, with the pilot flame only on, exhaust fan only on, bulk flow on and various combinations of these (Rajaram 2007). These results demonstrate that acoustic noise emissions exceed background noise by at least 10 dB for $\sim 150\,\mathrm{Hz} < f < 30\,\mathrm{kHz}$.

Images were obtained with a Phantom high-speed video camera, sensitive to light in both the visible and infrared spectrum. The camera was situated approximately

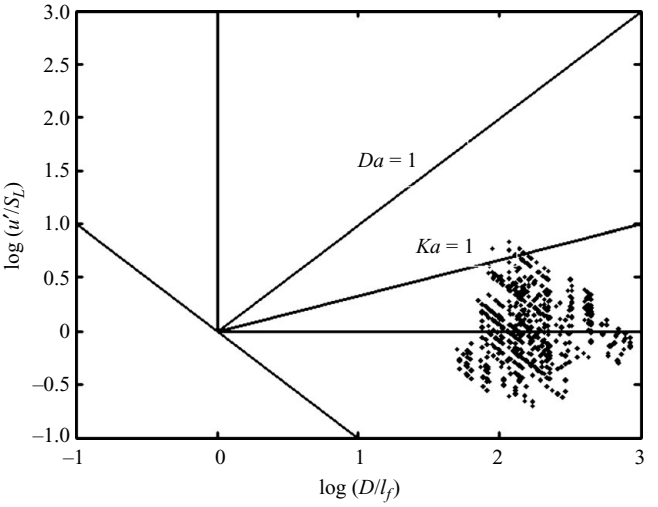

FIGURE 9. Location of test points on Borghi diagram, where l_F denotes calculated flame thickness.

1.2 m to the side of the burner, positioned vertically at roughly half the maximum flame height for a given burner. A Schott BG-38 filter (transmits more than 90 % between 360 nm and 575 nm) was used to cut off long and short wavelength emissions, including infra-red wavelengths. The captured light emissions include chemiluminescence from the typical dominant sources in hydrocarbon flames (Lee & Santavicca 2003), i.e. CH^* (390 and 430 nm), $C_2{}^*$ (510 nm) and $CO_2{}^*$ (continuum background from 300–600 nm), with the exception of OH^* (310 nm). The filter primarily cuts out black body radiation and signals from H_2O bands over 600 nm.

Chemiluminescence emissions from these species are good indicators of the flame zone (spatial errors are on the order of the flame thickness) and are known to be good indicators of the local heat release, within certain limitations as discussed in the literature (Lee & Santavicca 2003). Since the camera gathers light along the line of site, the radial and azimuthal characteristics of the instantaneous heat release distribution cannot be determined. However, by radially integrating these images, instantaneous data on the axial distribution of heat release can be determined. Since the flames have high aspect ratios (i.e. $L_{flame} \gg D$), this is the most physically interesting quantity from an acoustic emissions perspective, as shown in the next section.

3. Source characterization and turbulent flame dynamics

The spatiotemporal dynamics of the heat release rate must be thoroughly understood and characterized in order to understand the sound emissions that they are ultimately responsible for generating. This section describes an analysis of high-speed chemiluminescence images at selected conditions and the key length/time scales.

This heat release and acoustic data were obtained from 530 test points obtained over a range of burner diameters (6.4–34.8 mm), exit velocities ($Re_D = 10\,000$–$32\,000$), turbulence intensities ($u'/S_L = 0.1$–7), fuels (acetylene, methane and propane) and equivalence ratios (0.4 or tip loss to 1.1 or flashback), see Rajaram's thesis for a full tabulation of these test conditions (Rajaram 2007). The test matrix points are plotted on a Borghi diagram in figure 9, showing that they primarily fall in the flamelet

	Case 1	Case 2
Fuel	Natural gas	Acetylene
Burner diameter (mm)	10.9	34.8
U_{ave} (m s^{-1})	21.8	9.7
Turbulence intensity (%)	1.5	8.5
ϕ	0.95	0.63

TABLE 1. Enumeration of conditions for Case 1 and Case 2.

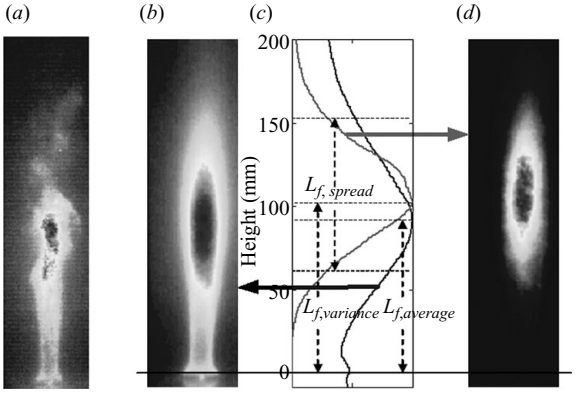

FIGURE 10. (*a*) Instantaneous image of the flame, (*b*) mean image, (*c*) radially integrated intensity of (*b*) and (*d*) as a function of height, (*d*) variance image.

regime. In addition, two test points were highlighted for more detailed comparisons of heat release and acoustic spectrum (see table 1 below).

Figure 10 shows a set of images obtained with a 10.9 mm, natural gas fuelled ($\phi = 0.95$) burner at an average nozzle exit velocity of 21.8 m s^{-1} and turbulence intensity of 1.5 %, referred to here as Case 1. A set of 32 768 frames were obtained at a recording rate of 2700 Hz at this condition. The left-most picture in figure 10(*a*) depicts an instantaneous image which, as expected, is asymmetric. As discussed earlier, this image is integrated over the line of sight, which precludes any analysis of radial/azimuthal variations, but allowing for analysis of transversely integrated axial distributions. The mean and variance of each pixel in the high-speed images for the above case is shown in figures 10(*b*) and 10(*d*). figure 10(*c*) plots axial distributions of the transversely integrated intensity images. This image indicates the location of maximum mean intensity, as well as the location of maximum fluctuations.

As there is an enormous amount of data in these images, it is necessary to extract reduced parameters that can be used to characterize the key flame characteristics. Three length scales are defined: first, $L_{f,average}$ is defined as the distance from the burner exit to the axial location where the horizontally integrated intensity of the mean image reaches a maximum. This is related to the mean flame length and is a function of flow velocity and turbulent flame speed. Second, $L_{f,variance}$ is the distance from the burner exit to the axial location where the horizontally integrated intensity of the variance image reaches a maximum. It can be anticipated that this length scale is more physically significant than $L_{f,average}$ in characterizing sound characteristics, as it is these fluctuations that are responsible for sound generation. Third, $L_{f,spread}$ is defined as the distance between the axial locations where the transversely integrated

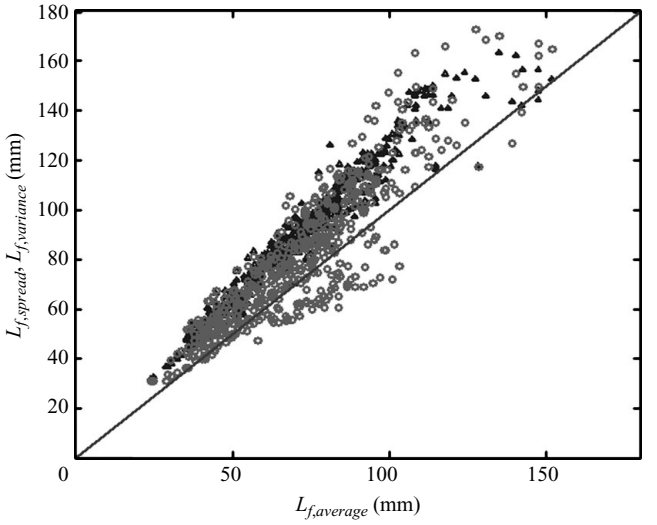

FIGURE 11. Measured relationship between flame length scales $L_{f,average}$ and $L_{f,variance}$ (Δ) and $L_{f,spread}$ (o) for entire database reported here.

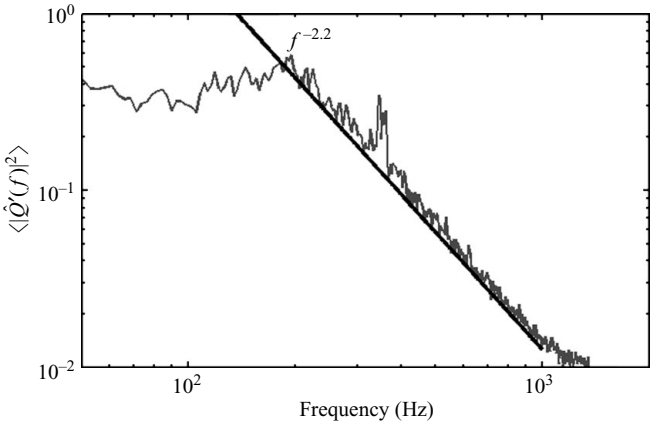

FIGURE 12. Spectrum of the spatially integrated heat release measurements measured at Case 1.

intensity of the variance image crosses 25 % of the maximum value. This length scale characterizes the axial size of the source region. These three characteristic lengths are illustrated in figure 10.

Figure 11 compares these three length scales for all conditions investigated in this study. It can be seen that the parameters are correlated with each other, but are not identical. This suggests that, under certain circumstances, these lengths can be used interchangeably to correlate data. However, each length scale controls different features of the problem, as discussed below.

Temporal characterization of these high speed movies were obtained by dividing the image sets into ensembles of 1024 images with 50 % overlap, yielding a spectral bin width of 2.6 Hz. Cross-spectral and coherence characteristics are determined with respect to the pixel of maximum intensity at that frequency. Figure 12 shows a typical spectrum of the spatially integrated chemiluminescence oscillations for Case 1. At low

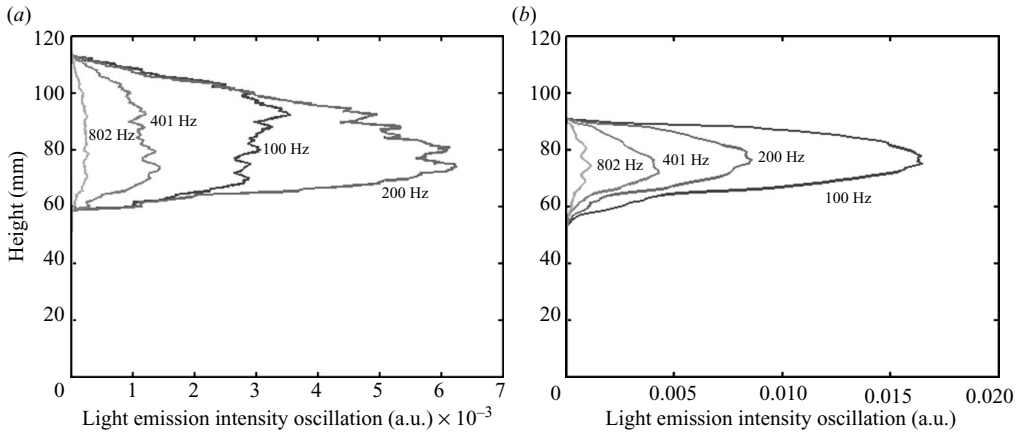

FIGURE 13. Axial variation of intensity oscillation at several frequencies for Case 1 (*a*) and Case 2 (*b*).

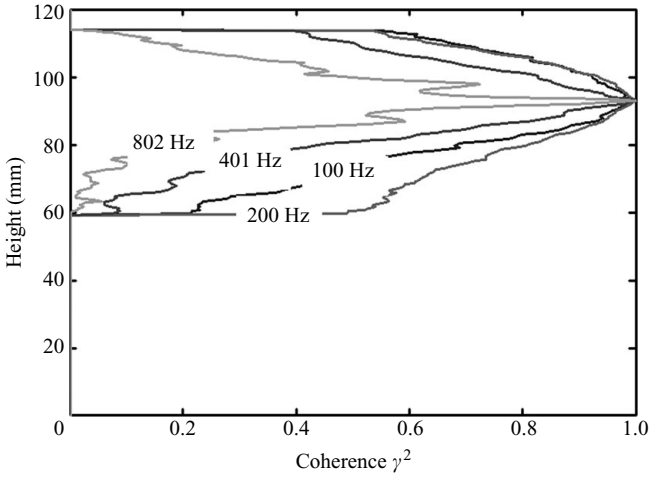

FIGURE 14. Axial variation of coherence with respect to the location of maximum intensity oscillation for Case 1.

frequencies, it has a fairly flat dependence upon frequency, while rolling off at higher frequencies as $f^{-2.2}$; we will return to this spectrum in the next section in order to compare it with the measured acoustic emissions.

Each individual image was radially integrated, reducing the flame analysis into a one-dimensional problem. Only pixels whose variance exceeds 50 % of the maximum variance value were used for this calculation, in order to focus upon the source region. Results are illustrated for two cases, Case 1 described above and Case 2, obtained with a 34.8 mm, acetylene fuelled ($\phi = 0.63$) burner at an average nozzle exit velocity of 9.7 m s^{-1} and turbulence intensity of 8.5 %.

The axial variation in intensity at several frequencies is plotted in figure 13, showing the spatial distribution of the heat release oscillations and the roll-off in amplitude at higher frequencies. Figure 14 plots the axial variation of the coherence $\gamma^2(y_1, f)$, showing that the size of the coherence region decreases with frequency. This trend can be illustrated by defining a frequency dependent coherence length scale $L_{f,coherence}(f)$.

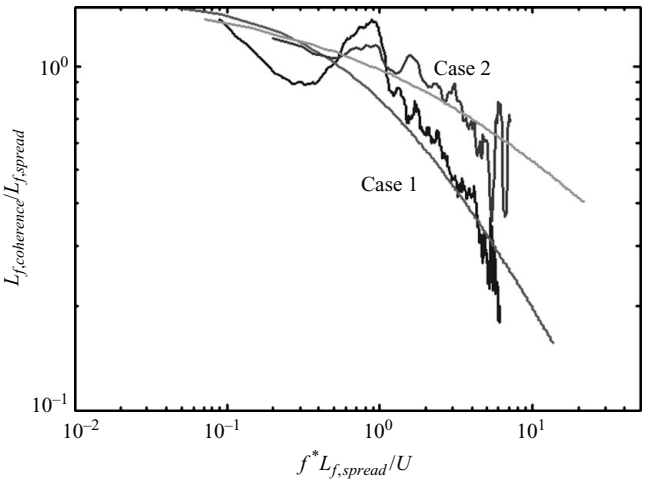

FIGURE 15. Dependence of $L_{f,coherence}$ upon frequency for Case 1 and Case 2. Best fits are defined by (3.2), using coefficients $n = 0.85$ and 0.5, $f_{cutoff} = 200$ and 340 Hz for Case 1 and 2, respectively.

This length scale is determined by fitting these curves to the equation

$$\gamma^2(y_1, f) = e^{-((y-L_{f,\mathrm{variance}}(f))/L_{f,coherence}(f))^2}. \tag{3.1}$$

The frequency dependence of $L_{f,coherence}(f)$ is illustrated in figure 15, showing the drop in coherence length with increasing frequency referred to above. Also shown on the line are curve fits of the form

$$L_{f,coherence}(f) = C\frac{L_{f,spread}}{1 + (f/f_{cutoff})^n}, \tag{3.2}$$

where C, f_{cutoff} and n are empirical constants. For both cases, the value of n is less than unity, implying that the coherence length drops slower than the frequency itself, a result that has important implications on the high-frequency emissions of the flame.

Consider next the cross-spectrum phase of the transversely integrated images φ. Although not shown (see Rajaram 2007), the phase φ varies linearly with frequency and axial distance, showing that the heat release fluctuations are propagating downstream in the axial direction at a constant velocity denoted as $U_{convection}$. This convection velocity can be obtained from the equation

$$U_{convection} = \left|\frac{\partial^2\varphi}{\partial f\,\partial y}\right|^{-1}. \tag{3.3}$$

Figure 16 plots the dependence of this estimated convection velocity upon the mean nozzle exit velocity, showing that they are nearly equal.

Taken together, these coherence/cross-spectrum magnitude and phase results show that the heat release fluctuations roll off in magnitude with increasing frequency, are convecting downstream at a velocity approximately equal to the nozzle exit velocity, and are correlated over a length scale that decreases with frequency. These behaviours are all expected as shown next. The roll off in heat release amplitude with increases in frequency are due to the low-pass filter character of the flame sheet itself (note that the G-equation describing the flame sheet dynamics is first order in time). For example, Boyer and Quinard's linear analysis shows that a flame sheet perturbed

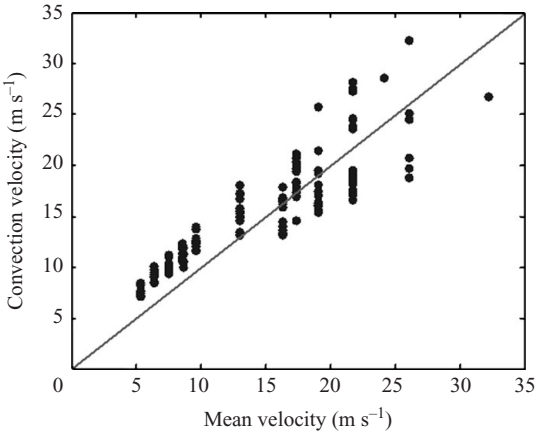

FIGURE 16. Comparison between axial propagation velocity of heat release disturbances, as estimated from cross-spectrum, and the mean nozzle exit velocity U_{ave}.

by a spectrally white velocity spectrum has an amplitude response that decays with frequency as f^{-2} (Boyer & Quinard 1990).

The constant convection velocity phase behaviour of the cross-spectrum, where $U_{convection} \approx U_{ave}$ is associated with the mean velocity component tangential to the flame surface. As shown by Boyer & Quinard (1990), tangential flow causes disturbances on the flame sheet to be convected at the mean velocity component tangential to the front. Related points have been recently emphasized by Driscoll (2008), who notes that convection of wrinkles along the flame by the tangential component of the flow velocity influences the turbulent flame speed.

Finally, the roll-off in coherence length of the heat release fluctuations along with increases in frequency is due to two effects. First, disturbances on the flame sheet are progressively reduced in magnitude by the smoothing action of flame propagation normal to itself as they convect downstream, i.e. 'kinematic restoration' (Law & Sung 2000; Peters 2000). In addition, the coherence length of the velocity disturbances exciting the flame decreases with frequency as well.

As will be shown next, these spatiotemporal characteristics of the heat release have important influences upon acoustic emissions. Utilizing Eq. 1.2 and following Dowling (in Crighton *et al.* 1992), the power spectrum of the acoustic pressure in the far field, defined as $\hat{P}(f,\vec{x}) = \langle|\hat{P}(f,\vec{x})|^2\rangle$, is given by

$$\hat{P}(f,\vec{x}) = \frac{(\gamma-1)^2}{4|\vec{x}|^2 c_0^4} f^2 \int\int \langle \hat{q}^*(\vec{y}_a, f)\hat{q}(\vec{y}_b, f)\rangle e^{ik_0\vec{x}\cdot(\vec{y}_b-\vec{y}_a)/|\vec{x}|}\, d\vec{y}_a\, d\vec{y}_b. \tag{3.4}$$

The $e^{ik_0\vec{x}\cdot(\vec{y}_b-\vec{y}_a)/|\vec{x}|}$ term in this equation describes retarded times due to both the axial and transverse distribution of the heat release (Lieuwen *et al.* 2006). Because the flame height is much greater than its width, the retarded time due to the transverse distribution of the flame is negligible except for very high frequencies, i.e. for $f > \sim 1500$ and 7500 Hz for the 34.8 and 6.7 mm burners, respectively. As such, this retarded time is simplified to $e^{ik_0(y_{1,b}-y_{1,a})\cos\theta}$, where θ is the polar angle shown in figure 1. Furthermore, defining the transversely integrated unsteady heat release, the same quantity reported in the measurements above, as $\widehat{q}_1$:

$$\widehat{q}_1(y_1, f) = \int \hat{q}(\vec{y}, f)\, dy_2\, dy_3. \tag{3.5}$$

Finally, define the axial distance between the two points in the source region as $\Delta = y_{b,1} - y_{a,1}$, and suppressing the subscript 'a' in y_1 yields

$$\hat{P}(f,\vec{x}) = \frac{(\gamma-1)^2}{4|\vec{x}|^2 c_0^4} f^2 \int\int \langle \hat{q}_1^*(y_1, f)\hat{q}_1(y_1+\Delta, f)\rangle \mathrm{e}^{-\mathrm{i}k_0\Delta\cos\theta}\,\mathrm{d}y_1\,\mathrm{d}\Delta. \tag{3.6}$$

Using the definition of coherence and cross-spectrum,

$$\gamma^2(y_1, y_1+\Delta, f) = \frac{|\langle \hat{q}_1^*(y_1, f)\hat{q}_1(y_1+\Delta, f)\rangle|^2}{\langle|\hat{q}_1(y_1, f)|^2\rangle\langle|\hat{q}_1(y_1+\Delta, f)|^2\rangle}. \tag{3.7}$$

Since the heat release fluctuations phase linearly vary with axial distance as shown earlier, the cross-spectrum term can be written as

$$\langle \hat{q}_1^*(y, f)\hat{q}_1(y_1+\Delta, f)\rangle = \langle|\hat{q}_1(y_1, f)|^2\rangle^{1/2}\langle|\hat{q}_1(y_1+\Delta, f)|^2\rangle^{1/2} \times |\gamma(y_1, y_1+\Delta, f)|\mathrm{e}^{-2\pi\mathrm{i}f\Delta/U_{ave}}. \tag{3.8}$$

As such, (3.6) can be written as

$$\hat{P}(f,\vec{x}) = \frac{(\gamma-1)^2}{4|\vec{x}|^2 c_0^4} f^2 \int\int \langle|\hat{q}_1(y_1, f)|^2\rangle^{1/2}\langle|\hat{q}_1(y_1+\Delta, f)|^2\rangle^{1/2} \times |\gamma(y_1, y_1+\Delta, f)|e^{-2\pi i f\Delta/U_{ave}(1+M\cos\theta)}\,\mathrm{d}y_1\,\mathrm{d}\Delta \tag{3.9}$$

Or, by non-dimensionalizing length scales by $L_{f,spread}$, denoting dimensionless quantities with a tilda (~), and defining $St = fL_{f,spread}/U_{ave}$ and $M = U_{ave}/c_o$:

$$\hat{P}(f,\vec{x}) = \frac{(\gamma-1)^2 M^4 St^2}{|\vec{x}|^2 U_o^2} \int\int \langle|\hat{q}_1(\tilde{y}_1, f)|^2\rangle^{1/2}\langle|\hat{q}_1(\tilde{y}_1+\tilde{\Delta}, f)|^2\rangle^{1/2} \times |\gamma(\tilde{y}_1, \tilde{y}_1+\tilde{\Delta}, f)|\mathrm{e}^{-2\pi\mathrm{i}St\tilde{\Delta}(1+M\cos\theta)}\,\mathrm{d}\tilde{y}_1\,\mathrm{d}\tilde{\Delta}. \tag{3.10}$$

Note that the relationship between the spectral characteristics of the acoustic emissions and heat release depend upon four quantities: Strouhal number, Mach number, spatial variation of the heat release and coherence length scale. In most instances, the Mach number correction is quite small (see Lieuwen *et al.* 2006), reducing this parameter set to three. The properties of the spectrum can be worked out for various limiting values of these parameters. The reader is referred to Leppington's chapter (Crighton *et al.* 1992) for an overview of the asymptotic methods used to obtain the limits quoted below.

The low Strouhal number limit is the simplest. If it is assumed that $St \ll 1$ and that $|\gamma(\tilde{y}_1, \tilde{y}_1+\tilde{\Delta}, f)| \sim O(1)$ (A more precise description of this limit is that the coherence or $\tilde{L}_{f,coherence}$ normalized by some reference value in the Strouhal range of interest must be $O(1)$. The key constraint on the coherence for evaluating this particular asymptotic limit is that remain a weak function of frequency.), then

$$St \ll 1,\ \tilde{L}_{f,coherence} \sim O(1) :\ \hat{P}(f,\vec{x}) \sim St^2\langle|\hat{Q}'(St)|^2\rangle, \tag{3.11}$$

where $\langle|\hat{Q}'(f)|^2\rangle = \langle|\int \hat{q}_1(\tilde{y}_1, f)\,\mathrm{d}\tilde{y}_1|^2\rangle$ is equal to the power spectrum of the total spatially integrated heat release, a quantity that was experimentally determined in this study, e.g. see figure 12.

The high Strouhal limit is more subtle and depends upon the relative values of the convective wavelength U_{ave}/f and the coherence length scale $L_{f,coherence}$ (see (3.2)), i.e. upon the value of $St\tilde{L}_{f,coherence}$. These two quantities are contained in terms that

exponentially decrease and oscillate with increases in frequency, exerting different asymptotic tendencies on (14).

We first consider the short coherence length scale limit. If $St\ \tilde{L}_{f,coherence} \ll 1$ and $\tilde{L}_{f,coherence} \ll 1$, then

$$\hat{P}(St, \vec{x}) \sim St^2 \tilde{L}_{f,coherence} \int \langle |\hat{q}_1(\tilde{y}_1, f)|^2 \rangle \, \mathrm{d}\tilde{y}_1 \sim St^2 \tilde{L}^2_{f,coherence} \langle |\hat{Q}'(St)|^2 \rangle. \tag{3.12}$$

This $St\ \tilde{L}_{f,coherence} \ll 1$ limit requires that the coherence length scale decay faster with frequency/Strouhal number than f^{-1}. For our data, this is not the case, as shown in figure 15, and so is not pursued further; however, such a limit might be of interest for some other system.

The last limit, $St\ \tilde{L}_{f,coherence} \gg 1$, requires asymptotic methods for highly oscillatory integrals. Such fast oscillation integrals are dominated by the characteristics of the integrand kernel,

$$\psi(\tilde{y}_1, \tilde{\Delta}, f) = \langle |\hat{q}_1(\tilde{y}_1, f)|^2 \rangle^{1/2} \langle |\hat{q}_1(\tilde{y}_1 + \tilde{\Delta}, f)|^2 \rangle^{1/2} |\gamma(\tilde{y}_1, \tilde{y}_1 + \tilde{\Delta}, f)|, \tag{3.13}$$

near the *boundaries* of the integration domain (e.g. at $y = 60$ and 115 mm for the data shown in figure 13*a*), more precisely over the dimensionless length scale $1/St$. For example, the high-frequency limit of the following integral can be expanded in inverse powers of the Strouhal number as

$$\lim_{St\to\infty} \int_a^b q(x) \mathrm{e}^{-2\pi \mathrm{i} St x} \, \mathrm{d}x = \underbrace{\frac{\mathrm{i}}{2\pi St} \left(q(b) \mathrm{e}^{-2\pi \mathrm{i} St b} - q(a) \mathrm{e}^{-2\pi \mathrm{i} St a} \right)}_{O(1/St)} + \underbrace{\frac{1}{(2\pi St)^2} \left(\frac{\mathrm{d}q(b)}{\mathrm{d}x} \mathrm{e}^{-2\pi \mathrm{i} St b} - \frac{\mathrm{d}q(a)}{\mathrm{d}x} \mathrm{e}^{-2\pi \mathrm{i} St a} \right)}_{O(1/St^2)} + O(1/St^3). \tag{3.14}$$

For the double integral of interest here, these leading order terms are squared, so the expansion is in terms of $1/St^2$, $1/St^4$ and so forth. These terms are then multiplied by the St^2 term (see 3.10), leading to terms of $O(1)$ and $O(1/St^2)$ as shown below:

$$\hat{P}(f, \vec{x}) \sim St^2 \int\int \psi(\tilde{y}_1, \tilde{\Delta}, f) \mathrm{e}^{-2\pi \mathrm{i} St \tilde{\Delta}} \, \mathrm{d}\tilde{y}_1 \, \mathrm{d}\tilde{\Delta} \sim \left[\psi(\tilde{y}_1, \tilde{\Delta}, f) \Big|_{\tilde{\Delta} = -\tilde{y}_1}^{\tilde{\Delta} = L - \tilde{y}_1} \right]_{\tilde{y}_1 = 0}^{\tilde{y}_1 = L} + O(1/St^2). \tag{3.15}$$

To summarize the above results, the spatiotemporal characteristics of the heat release influence the acoustic spectrum in fundamentally different ways, depending upon Strouhal number and coherence lengths scale; these are summarized in figure 17. For low frequencies, (or more precisely, in the $St \ll 1$, $|\gamma(\tilde{y}_1, \tilde{y}_1 + \tilde{\Delta}, f)| \sim O(1)$ limit), $\hat{P}(f, \vec{x})$ is independent of the spatial distribution of $\hat{q}_1(y_1, f)$. It is only the spatially integrated spectral characteristics of the heat release (multiplied by St^2) that control the acoustic spectrum, as summarized in (3.11). The $St\tilde{L}_{f,coherence} \gg 1$ is also largely independent upon the heat release distribution. However, here the characteristics of $\hat{q}_1(y_1, f)$ in the interior of the flame brush have no effect whatsoever. It is only its characteristics at the boundaries that matter in this case. While fig. 17 shows these relationships in general, a given system will cut through this space along some parametric curve with increasing frequency. This curve is indicated by the dashed lines in the figure for Case 1 and Case 2. This shows explicitly the asymptotic regimes

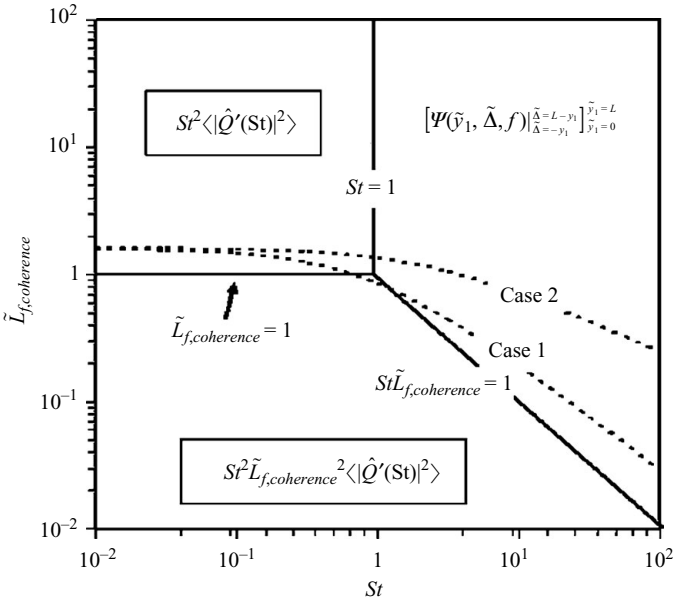

FIGURE 17. Summary plot of relationship between acoustic and heat release spectrum in various asymptotic regimes. Dashed lines indicate actual range of values for Case 1 and 2.

of interest for this configuration. These predictions are discussed further in the next section.

4. Acoustic data

4.1. *Acoustic inferences on source region characteristics*

This section presents results from the test matrix described in the prior section and presented in figure 9. One of the key features of attached flames, whether a Bunsen flame as considered here, or a bluff body or 'inverted V', is that the turbulent flame brush thickness grows with downstream distance. This leads to growing levels of heat release fluctuations with downstream distance from the flame attachment point. This necessarily implies that the acoustic source region is not uniformly distributed along the flame, but is concentrated downstream. This is in contrast to a freely propagating turbulent flame (e.g. see Lawn, Williams & Schefer 2005), where the flame brush thickness remains relatively constant along the flame.

While this point can be anticipated from figure 10, which shows that the largest fluctuations in heat release oscillations occur near the flame tip, it can also be directly inferred from the acoustic data. Two microphones located at different angles with respect to the burner axis, and equidistant from the burner exit centreline, will necessarily be different distances, and therefore acoustic travel times, from each spatial point in the flame region. This acoustic time delay between these two microphone measurements, $\tau_{acoustic}$, was estimated from the phase of the cross-spectrum for all 530 test points. This acoustic time delay was then compared to the time delay that would be expected if the noise were emitted from some virtual point downstream of the burner $\tau_{geometric} = (R_1 - R_3)/c$, where R_1 and R_3 denote the distances from this virtual point to microphones 1 and 3. Figure 18 shows that selecting this virtual point as coinciding with the burner centreline at a downstream axial distance of

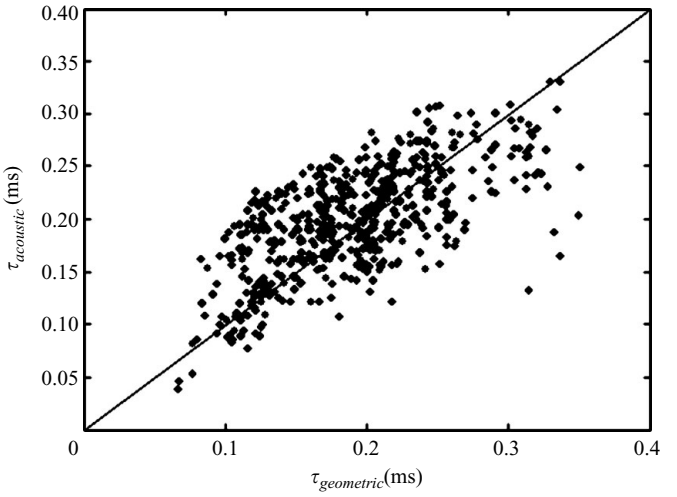

FIGURE 18. Comparison of time-lags calculated using cross spectrum, to the time lag calculated geometrically by assuming a source located at axial station of $L_{f,variance}$.

$L_{f,variance}$ leads to the same time delay as that measured acoustically. In other words, the time delay between the two microphone measurements is equal to that expected from the noise originating at the centrepoint of maximum light emission fluctuations. This affirms the point that the length scale $L_{f,variance}$, not $L_{f,average}$ (although this length scale would lead to a good correlation between $\tau_{geometric}$ and $\tau_{acoustic}$, their values would not be equal), controls the sound emissions characteristics of the flame.

The scatter in the data about the $\tau_{acoustic} = \tau_{geometric}$ line shown in figure 18 is to be expected based on the fact that the noise is not emitted at a single point, but is centred around this point over a distance characterized by $L_{f,spread}$. This spatial distribution of the unsteady heat release also influences the angular coherence of the combustion noise. The coherence of noise radiated at different angles from a randomly distributed noise source is a function of the ratio of the noise source coherence length and the acoustic wavelength (Rajaram 2007). Such angular coherence measurements have been used to decompose combustion/turbine ('core noise') and jet noise sources in jet engines (Krejsa 1983).

Figure 19(a) plots the dependence of the coherence between the 45° and 90° microphone data upon frequency for Case 1. It shows that the sound at these two locations is highly coherent up to about 1 kHz, then begins to roll off, though in a non-monotonic manner, and becomes essentially zero at about 4 kHz. This behaviour of the coherence function was characterized by a cut-off frequency f_{cutoff} defined as the frequency at which the coherence dropped to 0.75. Other definitions were also considered leading to similar results (Rajaram 2007).

$L_{fspread}$ can be used to correlate this cutoff frequency as shown in figure 19(b). This plot shows that f_{cutoff} scales inversely with $L_{f,spread}$. Thus, the frequency and/or wavenumber over which acoustic emissions remain coherent at two measurement points is directly correlated with the size of the source region. Although not shown, similar results were also obtained for the other microphone location pairs, showing that f_{cutoff} increases as the angle between the microphone pairs decreases, as expected (Rajaram 2007).

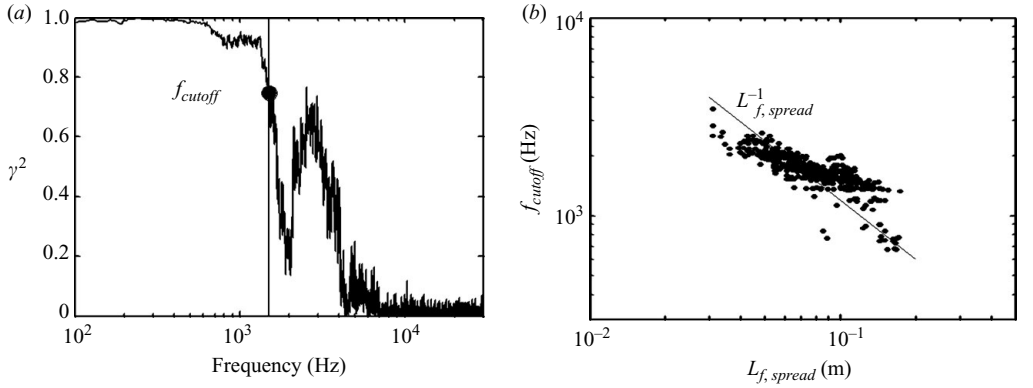

FIGURE 19. (*a*) Dependence of coherence between the microphones at 45° and 90° upon frequency and the illustration of the cutoff frequency definition, (*b*) dependence of the cutoff frequency upon $L_{f,spread}$ for the same microphone positions.

We next consider the spectral characteristics of the acoustic emissions. As noted in § 1, the acoustic spectra has a nearly universal shape that can be characterized by three regimes: a low frequency spectral dependence given by f^{β}, a peak in the spectra at f_{peak}, and the high-frequency spectral decay $f^{-\alpha}$. These three corresponding parameters, β, α and f_{peak} are considered in more detail next.

4.2. *Low frequency slope (β)*

To the best of our knowledge, the low-frequency acoustic spectrum has not been previously characterized in the literature. Accurate measurement of its characteristics is hindered by signal to noise problems, as this spectral range usually corresponds with regimes of high-background noise and also the undulations in the low frequency spectrum due to room reflection (see figure 5).

In order to reduce the effect of room reflections, only the cases with $f_{peak} > 600$ Hz were used to determine β. Given that room reverberation effects are significant at frequencies below ~ 200 Hz, this allowed a sufficient spectral range to estimate β. The resulting uncertainty in β is $\pm$ 0.3 at $f_{peak} = 600$ Hz and $\pm$0.1 at $f_{peak} = 1000$ Hz. The resulting estimate of β is plotted in figure 20, which shows it to have a nearly constant value of 2–2.4. This result can be understood from (3.11), which showed that the low-frequency side of the acoustic spectrum scales as $\hat{P}(f) \sim f^2 \langle |\hat{Q}'(f)|^2 \rangle$ (see figure 24). At low frequencies, $\langle |\hat{Q}'(f)|^2 \rangle$ has a roughly flat spectral profile (see figure 12). Hence we can expect a $\hat{P}(f) \sim f^2$ behaviour at low frequencies, at least to within the extent that the heat release spectrum is independent of frequency in this regime. The bias in β towards values of slightly greater than two is due to the fact that the spectrum of $\langle |\hat{Q}'(f)|^2 \rangle$ has a slightly positive slope at low frequencies. This point is demonstrated later in the context of figure 24, where it is shown that the ratio $\hat{P}(f)/\langle |\hat{Q}'(f)|^2 \rangle$ does indeed scale as f^2.

4.3. *Peak frequency*

From the solution of the wave equation discussed in the prior section (defined in (14)), the power spectrum is known to increase, then decrease with increases in frequency, having its maximum emissions at some frequency f_{peak}. This peak frequency is controlled by one of three processes, as can be seen from analysis of (3.10):

(i) Spectral character of the heat release $\hat{Q}'(f)$, which serves as the acoustic excitation.

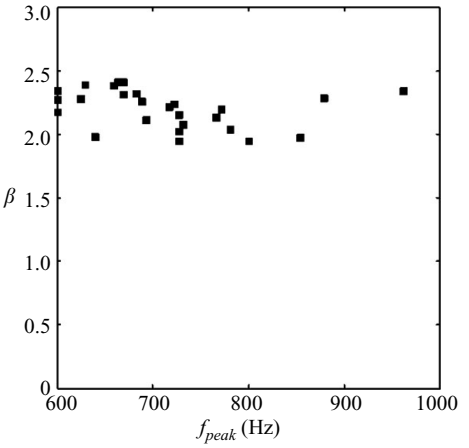

FIGURE 20. Dependence of low frequency decay exponent (β) upon f_{peak} for acetylene-air mixtures in the 6.4 mm burner

The other two processes are associated with the flame transfer function relating these heat release fluctuations to acoustic emissions, that is controlled by either:

(ii) Frequency dependence of the heat release correlation length, $|\gamma(\tilde{y}_1, \tilde{y}_1 + \tilde{\Delta}, f)|$,

(iii) Cancellation associated with the convection of the heat release disturbances along the flame, given by the term $e^{-2\pi i St\tilde{\Delta}}$.

While, in general, any one of these processes could potentially be controlling, it is this third one that is dominant for the flames considered here.

Consider first the unsteady heat release spectrum. As shown by (3.11), the acoustic spectrum for a flame with no convective cancellation and where the heat release disturbances remain correlated (i.e. $St \ll 1, \tilde{L}_{f,coherence} \sim O(1)$) is given by $\hat{P}(f, \vec{x}) \sim St^2\langle|\hat{Q}'(St)|^2\rangle$. As such, the spectrum could increase, peak and roll off due to the multiplication of the spectrum by St^2, due to the fact that the heat release is spectrally flat at low frequencies, and rolls off at higher frequencies (see figure 12). However, the heat release spectrum must roll off much faster than f^{-2} in order to cause the acoustic emissions to roll off. Our measurements indicate that the heat release spectrum rolls off at a decay rate just slightly larger than 2, e.g. it rolls off at a decay rate as $f^{-2.2}$ in figure 12. Thus, while not important here, this effect could potentially be controlling in situations where the heat release roll-off is much greater than f^{-2}.

The second effect, the reduction in coherence length scale with frequency is another potential mechanism for the peaking, then roll-off of the spectrum. As alluded to earlier, for this effect to dominate the cancellation effect, the coherence length scale must decay faster with frequency/Strouhal number than f^{-1}. Again, while it is possible that this could occur in other configurations, this is not the case in our facility where decay rates are slower than f^{-1}.

The third effect is the dominant one. It simply reflects the fact that convection of heat release oscillations downstream leads to cancellation of heat release oscillations from one point of the flame to the next due to time delays. This cancellation effect is captured by the Strouhal number St, and leads to a very simple scaling in this case, namely, that f_{peak} should directly scale with St.

To demonstrate that this is the case, figure 21 plots f_{peak} as a function of $U_{ave}/L_{f,spread}$. It was determined for all points in the data set by fitting a fourth

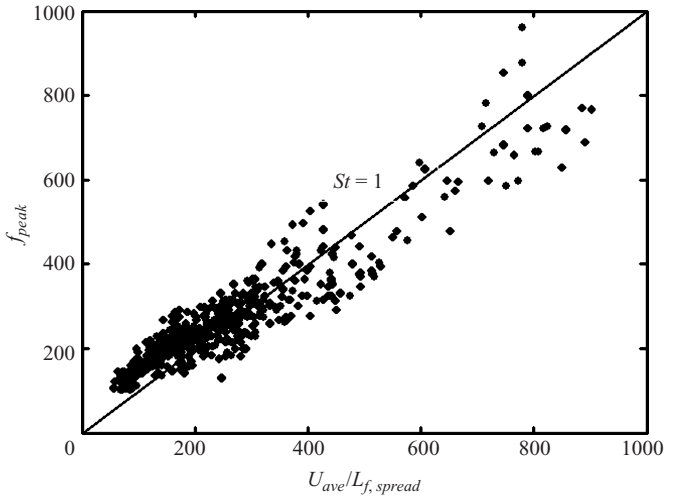

FIGURE 21. Strouhal number dependence of the peak frequency.

order polynomial curve through the acoustic spectrum near the peak. This procedure minimized the effects of small ripples in the spectrum (e.g. see figure 5) upon the estimate of f_{peak}. The resulting uncertainty in f_{peak} is approximately ± 30 Hz for $f_{peak} < 400$ Hz and ± 10 Hz at higher frequencies.

Figure 21 clearly shows that the f_{peak} data fall onto the $St = 1$ line. A similar scaling using a mean flame length (corresponding roughly to $L_{f,average}$ here, which is also correlated with the more physically significant parameter $L_{f,spread}$, see figure 11) has also recently been shown by Winkler *et al.* (2005) in a swirling flame.

This result shows that f_{peak} most fundamentally scales with $L_{f,spread}$ and U_{ave}. The dependence of f_{peak} upon other parameters proposed in prior studies (see Introduction) is apparently a manifestation of their influence upon these two parameters. For example, turbulence intensity (Strahle & Shivashankara 1974; Strahle 1983) does impact f_{peak} indirectly, through its impact on turbulent flame speed and, therefore, flame length. Also, the dependence of f_{peak} upon fuel/air ratio, interpreted by some as suggesting a chemical kinetic scaling of f_{peak}, is also simply a reflection of the influences of kinetic properties upon flame speed, and therefore the fundamentally significant flame length parameters.

Given this very simple f_{peak} scaling, and the controversy that has existed in the literature on this scaling for the last two decades, it is worth commenting on the conclusions from prior studies in the light of this result. We believe that there are two key reasons this scaling has not been noted earlier:

First, is the limited range of achievable L_f/U_{ave} values. Variations in flow velocity U_{ave} cause corresponding changes in flame length L_f that cause their ratio L_f/U_{ave} to essentially remain constant. This can lead to the erroneous conclusion that f_{peak} does not scale with U_{ave}. As such, probably the best way to vary L_f/U_{ave} is through changes in flame speed at constant U_{ave}. However, obtaining large variations in flame speed with a single fuel is difficult, because flame stability must also be maintained. For example, in the authors' prior publication (Rajaram & Lieuwen 2003), only one fuel was utilized and, because of the requirement to maintain a stable flame, the laminar flame speed could only be varied by about 30 %. As such, multiple fuels are

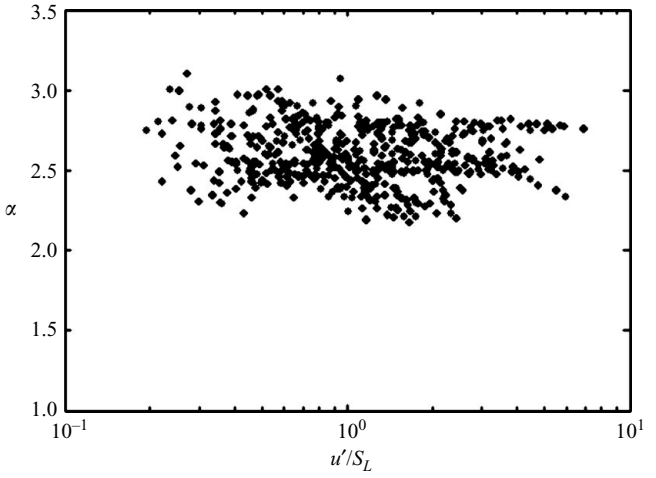

FIGURE 22. Dependence of high frequency slope parameter α upon turbulence intensity (measured at the jet exit centreline).

needed to expand this range. In the present work, results were also obtained with propane and acetylene, allowing S_L variations by a factor of 4.

The second reason is signal to noise issues and room reverberation effects. Except for very small burner diameters and very high flame speed mixtures, combustion noise generally peaks in the 100–400 Hz region where it is difficult to obtain anechoic conditions with low background noise. Given the relatively small movement of peak frequency that was likely present in many prior data sets due to the limited variations in L_f/U_{ave}, the underlying trend would be masked. This point can be appreciated by consideration of the variation in spectra with equivalence ratio in Rajaram, Preetham & Lieuwen (2005) and noting the problems associated with estimating f_{peak} due to room reverberation induced ripples.

4.4. *High frequency slope (α)*

We last consider the characteristics of the measured high-frequency acoustic emissions, parameterized by fitting the high frequency acoustic emissions to the power law $f^{-\alpha}$. Figure 22 compiles the resulting estimates for α. The correlation coefficient of the logarithm of the acoustic data with frequency exceeded 0.97 for all these points. The figure shows that α ranges in value from $\alpha = 2.1$–3.2. This range in values is consistent with the range measured by Belliard (1997) ($2.2 < \alpha < 3.4$), as well as Abugov & Obrezkov (1978) ($\alpha = 2.5$) and the theoretical prediction of Clavin & Siggia (1991) for the high u'/S_L limit ($\alpha = 5/2$).

The measured value of α can be compared to theoretical predictions for Cases 1 and 2. The asymptotic analysis suggested that the acoustic spectrum and heat release spectrum are directly related (i.e. without any additional St multiplicative terms, as are present in the low St limit). To illustrate that these predictions are consistent with the data, figure 23 compares the spectrum of heat release oscillations for Case 1 with its corresponding acoustic spectrum. The figure clearly shows that the roll off rates of the heat release spectrum is equal to that of the acoustic spectrum. This discussion suggests that the range in α values shown in figure 22 similarly reflects the variations in heat release spectrum encountered over the range of investigated conditions.

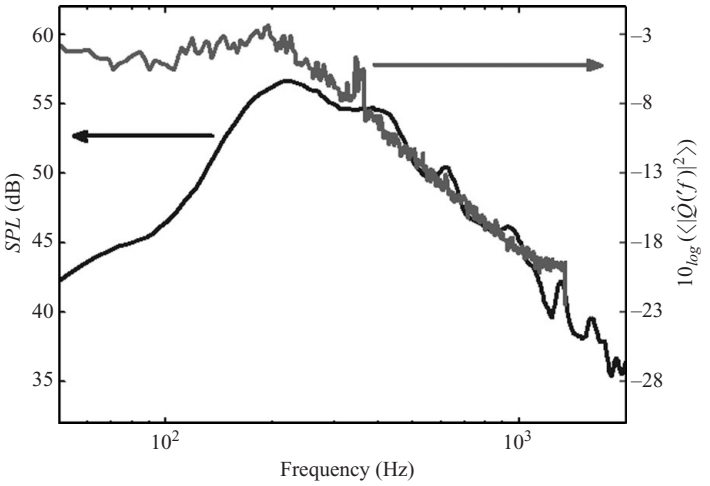

FIGURE 23. Comparison of spectrum of heat release fluctuations to the acoustic spectrum for Case 1.

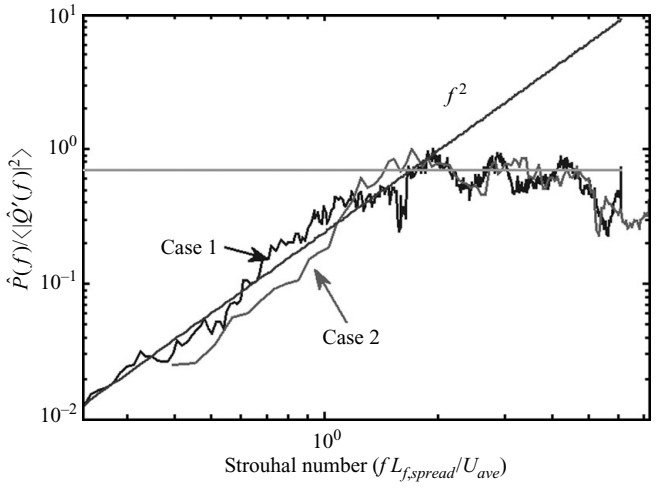

FIGURE 24. Comparison of ratio of acoustic and heat release spectrum $\hat{P}(f)/\langle|\hat{Q}'(f)|^2\rangle$ for Case 1 and Case 2.

The relationship between acoustic and heat release spectra over the entire frequency range can be better seen in figure 24, which plots the ratio $\hat{P}(f)/\langle|\hat{Q}'(f)|^2\rangle$, normalized by its maximum value for Cases 1 and 2. This figure clearly shows the high and low Strouhal number zones that determine this relationship. This ratio $\hat{P}(f)/\langle|\hat{Q}'(f)|^2\rangle$ has an f^2 dependence at low frequencies and becomes constant at higher frequencies. Both results are consistent with the predicted relationships between heat release and acoustic spectrum.

5. Concluding remarks

This paper has worked out the key spectral features of an anchored Bunsen flame, including its low-frequency and high-frequency characteristics and the scaling of the frequency of peak emissions. In addition, these characteristics have been

related to the underlying spectrum and spatiotemporal coherence characteristics of the unsteady heat release. An important feature of this investigated geometry is the anchored character of the flame in a high speed flow that is much greater than the turbulent flame speed. This leads to two important influences on the flame and its acoustic emissions. First, the flame brush grows downstream, leading to growing level of fluctuations in flame position and heat release rate with downstream distance. As such, the heat release fluctuations are not uniformly distributed in magnitude along the flame but grow with downstream distance. This leads to the concentration of the acoustic source region near the flame tip, as shown in the discussion of figure 18. This also leads to differences between the flame height and heat release fluctuation length scales, $L_{f,average}$ and $L_{f,variance}$. Second, due to the high-flow velocity relative to the flame speed, the flame is nearly parallel to the flow. This causes disturbances on the flame sheet to be convected at the mean velocity component tangential to the front. This behaviour plays an important role on the peak frequency scaling $St = f L_{f,spread}/Uo$ and the high-frequency scaling because of the phase cancellation term $e^{-2\pi i St\tilde{\Delta}}$ in (3.10).

A natural question for further consideration is what would be expected to remain the same and to change for other flame configurations. It appears that anchored flames, whether they are swirling, 'inverted V flames', or other shapes, will have similar character, e.g. they will also have a convective component to the heat release fluctuation, leading to coherence characteristics described in (3.8) and, therefore, a similar scaling for f_{peak}. This conclusion is supported by the measurements of Sattelmayer's group (e.g. see Winkler *et al.* 2005), who have demonstrated nearly identical scalings for f_{peak} in an inverted swirl flame. Furthermore, all flames apparently have the same $St \ll 1$ character that is controlled by the spatially integrated heat release spectrum, given by (3.11).

Significant differences in high-frequency scaling can be anticipated between anchored and freely propagating flames, however, for the same reasons. For example, this would apply to flames in lower speed flows where the flame is normal to the flow, such as the configuration described by Lawn *et al.* (2005). Similarly, it would also apply to the radiation characteristics of the leading edge of low swirl burner stabilized or vortex breakdown stabilized flames. In these cases, the peak and high-frequency characteristics are not influenced by the convective phase cancellation term $e^{-2\pi i St\tilde{\Delta}}$, but rather by the other processes described earlier: heat release spectrum, coherence characteristics and, in addition, non-compactness effects (given by the $e^{-ik_0\Delta\cos\theta}$ term in (10).

This discussion suggests the need for additional studies of combustion noise from flames where other physical processes control the acoustic spectrum. In particular, at least three different configurations would be of interest: those without a strong tangential flow component, those where the heat release correlation length scale rolls off faster than f^{-1}, and those where the heat release spectrum rolls off with frequency much faster than f^{-2}.

This research was supported by the National Science Foundation under contracts CTS-0092535 and CBET-0651045; contract monitor Dr Phil Westmoreland.

REFERENCES

Abugov, D. I. & Obrezkov, O. I. 1978 Acoustic noise in turbulent flames. *Combust. Explos. Shock Waves* **14**, 606–612.

Ahuja, K. K. 2003 Designing clean jet-noise facilities and making accurate jet-noise measurements. *Intl J. Aeroacoust.* **2**, 371–412.

Aldredge, R. C. & Williams, F. A. 1991 Influence of wrinkled premixed flame dynamics on large scale, low intensity turbulent flow. *J. Fluid Mech.* **228**, 487–511.

Belliard, A. 1997 Etude Expérimentale de L'émission Sonore des Flammes Turbulentes. PhD Thesis, Universités d'Aix-Marseille, Marseille.

Boyer, L. & Quinard, J. 1990 On the dynamics of anchored flames. *Combust. Flame* **82**, 51–65.

Bragg, S. L. 1963 Combustion noise. *J. Inst. Fuel* **36**, 12–16.

Briffa, F. E. J., Clark, C. J. & Williams, G. T. 1973 Combustion Noise. *J. Inst. Fuel* **46**, 207–216.

Chiu, H. H. & Summerfield, M. 1973 Theory of combustion noise. *Tech. Rep.* 1136. Princeton University.

Cho, J. H. & Lieuwen, T. 2005 Laminar premixed flame response to equivalence ratio oscillations. *Combust. Flame* **140**, 116–129.

Clavin, P. 2000 Dynamics of combustion fronts in premixed gases: from flames to detonations. *Proceeding of the Combustion Institute*, Pittsburgh, PA, pp. 569–585.

Clavin, P. & Siggia, E. D. 1991 Turbulent premixed flames and sound generation. *Combust. Sci. Technol.* **78**, 147–155.

Crighton, D. G., Dowling, A. P., Ffowcs Williams, J. E., Heckl, M. & Leppington, F. G. 1992 *Modern Methods in Analytical Acoustics.* Springer.

Cumpsty, N. A. 1979 Jet engine combustion noise: pressure, entropy and vorticity perturbations produced by unsteady combustion or heat addition. *J. Sound Vib.* **66**, 527–544.

Doak, P. E. 1973 Analysis of internally generated sound in continuous materials. III. The momentum potential field description of fluctuating fluid motion as a basis for a unified theory of internally generated sound. *J. Sound Vib.* **26**, 91–120.

Dowling, A. P. 1979 *Mean Temperature and Flow Effects on Combustion Noise.* AIAA. Paper no. 1979-0590.

Driscoll, J. 2008 Turbulent premixed combustion: flamelet structure and its effect on turbulent burning velocity. *Prog. Energy Combust. Sci.* **34**, 91–134.

Giammar, R. D. & Putnam, A. A. 1972 Combustion roar of premix burners, singly and in pairs. *Combust. Flame* **18**, 435–438.

Hassan, H. A. 1974 Scaling of combustion-generated noise. *J. Fluid Mech.* **66**, 445–453.

Huff, R. G. 1986 Theoretical prediction of the acoustic pressure generated by turbulence-flame front interactions. *J. Vib. Acoust. Stress Reliab. Des.* **108**, 315–321.

Ihme, M., Pitsch, H. & Bodony, D. 2006 Prediction of combustion generated noise in non-premixed turbulent jet flames using large eddy simulation. *AIAA Paper* 2006–2614.

Ihme, M., Pitsch, H. & Bodony, D. 2009 Radiation of noise in turbulent non-premixed flames. *Proc. Combust. Inst.* **32**, Pittsburgh, PA, pp. 1545–1553.

Kerstein, A. R. 1988 Fractal dimension of turbulent premixed flame. *Combust. Sci. Technol.* **60**, 441–445.

Kilham, J. K. & Kirmani, N. 1979 The effect of turbulence on premixed flame noise. *Proceeding of the* Combustion *Institute*, Pittsburgh, PA, pp. 327–336.

Kotake, S. 1975 On combustion noise related to chemical reactions. *J. Sound Vib.* **42**, 399–410.

Kotake, S. & Takamoto, K. 1987 Combustion noise: effects of the shape and size of burner nozzle. *J. Sound Vib.* **112**, 345–354.

Kotake, S. & Takamoto, K. 1990 Combustion noise: effects of the velocity turbulence of unburned mixture. *J. Sound Vib.* **139**, 9–20.

Krejsa, E. A. 1983 Application of 3-signal coherence to core noise transmission. AIAA. Paper no. 1983-0759.

Kumar, R. N. 1975 *Further Experimental Results on the Structure and Acoustics of Turbulent Jet Flames.* AIAA. Paper no. 1975-0523.

Law, C. K. & Sung, C. J. 2000 Structure, aerodynamics, and geometry of premixed flamelets. *Prog. Energy Combust. Sci.* **26**, 459–505.

Lawn, C. J., Williams, T. C. & Schefer, R. W. 2005 The response of turbulent premixed flames to normal acoustic excitation. *Proc. Combust. Inst.* **30**, Pittsburgh, PA, pp. 1749–1756.

Lee, J. G. & Santavicca, D. 2003 Experimental diagnostics for the study of combustion instabilities in lean, premixed combustors. *J. Propuls. Power* **19**, 735–750.

Lieuwen, T., Mohan, S., Rajaram, R. & Preetham 2006 Acoustic radiation from weakly wrinkled premixed flames. *Combust. Flame* **144**, 360–369.

Lighthill, M. J. 1952 On sound generated aerodynamically. I. General theory. *Proc. R. Soc. Lond. Ser.* A – *Math. Phys. Sci.* **211**, 565–587.

Mahan, J. R. 1984 A critical review of noise prodiction models for turbulent, gas-fueled burners. *Tech. Rep.* Contractor Report 3803. NASA.

Marble, F. E. & Candel, S. M. 1977 Acoustic disturbance from gas non-uniformities convected through a nozzle. *J. Sound Vib.* **55**, 225–243.

Matalon, M. & Matkowsky, B. J. 1982 Flames as gasdynamic discontinuities. *J. Fluid Mech.* **124**, 239–259.

Muthukrishnan, M., Strahle, W. C. & Neale, D. H. 1978 Separation of hydrodynamic, entropy, and combustion noise in a gas turbine combustor. *AIAA J.* **16**, 320–327.

Petela, G. & Petela, R. 1983 Diagnostic possibilities on the basis of premixed flame noise levels. *Combust. Flame* **52**, 137–147.

Peters, N. 2000 *Turbulent Combustion*. Cambridge University Press.

Putnam, A. A. 1976 Combustion roar of seven industrial gas burners. *J. Inst. Fuel* **49**, 135–138.

Rajaram, R.2007 Characteristics of sound radiation from turbulent premixed flames. PhD Thesis, Georgia Institute of Technology, Atlanta.

Rajaram, R. & Lieuwen, T. 2003 Parametric studies of acoustic radiation from turbulent premixed flames. *Combust. Sci. Technol.* **175**, 2269–2298.

Rajaram, R., Preetham, P. & Lieuwen, T. 2005 *Frequency Scaling of Turbulent Premixed Flame Noise*. AIAA. Paper no. 2005-2828.

Ramohalli, K. N. R. & Seshan, P. K. 1983 Acoustic Emissions Reveal Combustion Conditions. AIAA. Paper no. 1983-076.

Roberts, J. P. & Leventhall, H. G. 1973 Noise sources in turbulent gaseous premixed flames. *Appl. Acoust.* **6**, 301–308.

Shivashankara, B. N. 1974 An experimental study of noise produced by open turbulent flames. PhD Thesis, Georgia Institute of Technology, Atlanta.

Shivashankara, B. N. 1978 Gas turbine core noise source isolation by internal-to-far-field correlations. *J. Aircr.* **15**, 597–600.

Shivashankara, B. N., Strahle, W. C. & Handley, J. C. 1975 Combustion noise radiation by open turbulent flames. *Prog. Astronaut. Astronaut.* **37**, 277–296.

Smith, T. J. B. 1961 Combustion noise. PhD Thesis, The University of Leeds, Leeds.

Smith, T. J. B. & Kilham, J. K. 1963 Noise generation by open turbulent flames. *J. Acoust. Soc. Am.* **35**, 715–724.

Stephenson, J. & Hassan, H. A. 1977 Spectrum of combustion-generated noise. *J. Sound Vib.* **53**, 283–288.

Strahle, W. C. 1983 Combustion noise source. *Proceedings - National Conference on Noise Control Engineering*, Poughkeepsie, NY, pp. 379–388.

Strahle, W. C. 1971 On combustion generated noise. *J. Fluid Mech.* **49**, 399–414.

Strahle, W. C. 1973 Refraction, convection and diffusion flame effects in combustion generated noise. *Proc. Combustion Institute* **14**, Pittsburgh, PA, pp. 527–535.

Strahle, W. C. 1978 Combustion noise. *Prog. Energy Combust. Sci.* **4**, 157–176.

Strahle, W. C. & Shivashankara, B. N. 1974 A rational correlation of combustion noise results from open turbulent premixed flames. *Proceeding of the* Combustion *Institute*, Pittsburg, PA, pp. 1379–1385.

Tam, C. & Auriault, L. 1999 Jet mixing noise from fine scale turbulence. *AIAA J.* **37**, 145–153.

Tam, C. K. W., Pastouchenko, N. N., Mendoza, J. & Brown, D. 2005 Combustion noise of auxiliary power units. AIAA. Paper no. 2005-2829.

Truffaut, J.-M., Searby, G. & Boyer, L. 1998 Sound emission by non-isomolar combustion at low mach numbers. *Combust. Theory Modelling* **2**, 423–428.

Videto, B. D. & Santavicca, D. A. 1991 A turbulent flow system for studying turbulent combustion process. *Combust. Sci. Technol.* **76**, 159–164.

Wang, H. Y., Preetham, Law, C. K. & Lieuwen, T. 2009 Linear response of stretch-affected premixed flames to flow oscillations. *Combust. Flame* **156**, 889–895.

Wäsle, J., Winkler, A. & Sattelmayer, T. 2005 Spatial coherence of the heat release fluctuations in turbulent jet and swirl flames. *Flow Turbul. Combust.* **75**, 29–50.

Winkler, A., Wäsle, J. & Sattelmayer, T. 2005 *Experimental Investigations on the Acoustic Efficiency of Premixed Swirl Stabilized Flames.* AIAA. Paper no. 2005-2908.